Dimensional Standard for Micro X-ray Computed Tomography

ARTICLE *in* ANALYTICAL CHEMISTRY · OCTOBER 2010

Impact Factor: 5.64 · DOI: 10.1021/ac101522q · Source: PubMed

2 AUTHORS:

Brian M Patterson
Los Alamos National Laboratory
85 PUBLICATIONS **331** CITATIONS
SEE PROFILE

Christopher E Hamilton
Los Alamos National Laboratory
35 PUBLICATIONS **542** CITATIONS
SEE PROFILE

Anal. Chem. **2010,** *82,* 8537–8543

Dimensional Standard for Micro X-ray Computed Tomography

Brian M. Patterson* and Christopher E. Hamilton

Materials Science and Technology Division, PO Box 1663, Los Alamos National Laboratory, Los Alamos, New Mexico 87545

The decrease in the cost of high end computing and the availability of high quality X-ray sources in the laboratory environment has led to an increased use of three-dimensional (3D) X-ray micro computed tomography (μCT). In the medical community, the primary concern for CT is calibrating for X-ray absorption and ascertaining the difference between healthy tissue and cancerous tissue or examining fractures. Absorption calibration is also important in the materials community, however confirming dimensional accuracy of voids, defects, machined parts, cracks, or the distribution of dispersed particles is typically more important. One key aspect of μCT that is often overlooked in the literature is the number of radiographs required for dimensional accuracy of the 3D reconstruction and minimization of image noise. In μCT, a number of radiographs are collected in theta increments as the sample is rotated at least 180°. They are typically collected in 1° increments (or 181 radiographs), 0.25° increments (721 radiographs), or some other multiple. The question that arises, especially in a laboratory based instrument, where the required exposure times are longer to get high-quality signal-to-noise compared to synchrotron sources, is what is the optimal number of images required to reach the volumetric statistics of the sample, and minimize the noise while not overly scanning the sample at a cost in time? A dimensional standard based upon NIST certified glass microspheres dispersed in a low density poly(styrene) matrix to answer this question is proposed. Experiments are shown that describe the microsphere size statistics as a function of number of radiographs calculated using a commercial software package, AvizoFire. These results are important in understanding the distribution of voids in a foam and confirming the accuracy of the 3D measurements obtained.

X-ray computed tomography (CT), first proposed in the early 1900′s but not implemented until the 1970s, is based upon a calculation of the projection images of X-ray radiography to generate a 3D rendering of an object. Key to implementation of this technology is the ability to process a multitude of X-ray radiographs and reconstruct them into a 3D cross section of the item of interest. X-ray CT is widely used in the medical field to examine the internal structure of the patient for defects (broken bones), extraneous growth (tumors) or other structures of interest. Medical CT, which operates on the 100 μm resolution scale is primarily interested in precise measurements of the X-ray absorption value of the tissue and limiting the X-ray exposure of the patient. Precise knowledge of the X-ray absorption value of a tissue is very important in correct diagnosis; spatial resolution is often of secondary importance.

Outside of the medical field, CT is also being employed increasingly within the materials science community. The ability to nondestructively examine internal features of experimental samples is useful for a suite of materials characteristics such as porous foam structures,[1−4] particle sizes,[5] manufacturing quality,[6−9] porosity[10−12] or void volume,[13] and metallic grain structure.[14,15] CT is used in a wide range of size scales from imaging of entire engine blocks down to single celled yeasts.[16,17] A very good treatise is available for the application of CT to geological materials.[18]

* To whom correspondence should be addressed. E-mail: bpatterson@lanl.gov.

(1) Montminy, M.; Tannenbaum, A. R.; Macosko, C. W. *J. Cell. Plast.* **2001**, *37*, 501–514.
(2) Montminy, M.; Tannenbaum, A. R.; Macosko, C. W. *J. Colloid Interface Sci.* **2004**, *280*, 202–211.
(3) Elmoutaouakkil, A.; Salvo, L.; Maire, E.; Peix, G. *Adv. Eng. Mater.* **2002**, *4* (10), 803–807.
(4) Haubrich, S. S. *Experimental Observations and Simulations of the Mechanical Deformation of Amorphous Metallic Foam*; Iowa State Univeristy: Ames, 2009.
(5) Lin, C. L.; Miller, J. D. *Powder Technol.* **2005**, *154*, 61–69.
(6) Park, H.; Miwa, K. *Mater. Trans.* **2003**, *44* (11), 2326–2333.
(7) Patterson, B. M.; Campbell, J.; Havrilla, G. J. *X-Ray Spectrom.* **2010**, *39* (3), 184–190.
(8) Huang, H.; Eddinger, S. A.; Schoff, M. *Fusion Sci. Technol.* **2009**, *55* (4), 373–379.
(9) Jaeggi, C.; Mooser, R.; Frauchinger, V.; Wyss, P. *Mater. Lett.* **2009**, *63*, 2643–2645).
(10) Ferreira, E. S. B.; Boon, J. J.; Scherrer, N. C.; Marone, F.; Stampanoni, M. *Proc. SPIE* **2009**, *7391*, 73910L).
(11) Dunsmuir, J. H.; Bennett, S.; Fareria, L.; Mingino, A.; Sansone, M. *Powder Diffr.* **2006**, *21* (2), 125–131.
(12) Dudek, M. A.; Hunter, L.; Kranz, S.; Williams, J. J.; Lau, S. H.; Chawla, N. *Mater. Charact.* **2010**, *61*, 433–439.
(13) Moritz, K.; Moritz, T. *J. Eur. Ceram. Soc.* **2010**, *30*, 1203–1209.
(14) Babout, L.; Ludwig, W.; Maire, E.; Buffiere, J. Y. *Nuc. Instrum. Methods Phys. Res., B* **2003**, *200*, 303–307.
(15) Ludwig, W.; King, A.; Reischig, P.; Herbig, M.; Lauridsen, E. M.; Schmidt, S.; Proudhon, H.; Forest, S.; Cloetens, P.; Rolland du Roscoat, S.; Buffiere, J. Y.; Marrow, T. J.; Poulsen, H. F. *Mater. Sci. Eng., A* **2009**, *524*, 69–76.
(16) Andrews, J. C.; Brennan, S.; Liu, Y.; Pianetta, P.; Almeida, E. A. C.; van der Meulen, M. C. H.; Wu, Z.; Mester, Z.; Ouerdane, L.; Gelb, J.; Feser, M.; Rudati, J.; Tkachuk, A.; Yun, W. *J. Phys.: Conf. Ser.* **2009**, *186*, 012081.
(17) Larabell, C. A.; Le Gros, M. A. *Mol. Biol. Cell* **2004**, *15*, 957–962.
(18) Ketcham, R. A.; WD, C. *Comput. Geosci.* **2001**, *27*, 381–400.

10.1021/ac101522q
Published on Web 09/16/2010

One variation of this technique is the micro X-ray computed tomography (μCT), which is used to image small objects at high resolution.[8,19,20] In the μCT unit, spatial resolution on the 1 μm scale (or even smaller) is commonplace. Key to this technology is the use of a micro focus X-ray source (~5 μm spot size), a high-resolution detector, and a high-performance computer processor. With the availability of stable micro focus sources, and the dramatic decrease in the cost of computing power, laboratory based μCT units are becoming more commonplace as demonstrated by the number of vendors (5+) offering commercial instrumentation. Laboratory based μCT units operate using a stationary source and detector with a rotation stage. Radiographs are collected by shining the X-rays through the sample which are projected onto a scintillator. The scintillator converts the X-ray photons into visible light that are then detected by a CCD. Specifically, in the Xradia system, the system utilized for the current investigation, a series of microscope objectives that magnify the visible photons before imaging by the CCD are used. To collect a 3D image of the sample, radiographic exposures are collected of each sample as it is rotated about the vertical axis. Typical exposure for each radiograph is 10−60 s and the number of radiographs may vary from ~100 to thousands.

In spite of the increasing demand for 3D data in the materials science community and the obvious role that CT can play in responding to this demand, there are a number of issues associated with its widespread and standardized use. A particularly important question to the materials science community, that is not examined in the literature, is the question of how many radiographs are required to generate a 3D rendering of the object such that the measured volume of an object (or void) and its dimensional variation will be independent of the tomographic method employed? This question is not only relevant to generating computationally efficient data sets, but also is critical for the materials science community as we move forward to employing CT methods in a standardized and time sensitive fashion. In this study, this specific question is examined.

EXPERIMENTAL SECTION

Dry borosilicate glass microspheres, 20 μm in diameter, embedded in poly(styrene) were used as a 3D dimensional size calibration standard, Figure 1A. The 20 μm microspheres have a certificate of analysis (NIST traceable); they are 17.3 μm ± 1.4 μm diameter with a 12 CV (12% relative standard deviation). These microspheres were chosen because of their small size in relation to the high-resolution objective's field of view and they are near the measured resolution of the instrument. They are only ~14 voxels wide. A voxel is the 3D equivalent of a pixel, a volume pixel. Because of their small size, the quality of the measurements should be highly dependent upon the number of radiographs used. Other sized microspheres are available from the manufacturer and should be chosen as appropriate for the resolution of the instrument and technique used.

The standard was prepared as follows: A mixture containing 0.1 g sorbitan monooleate (SMO, Lonzest), 0.13 g styrene, and

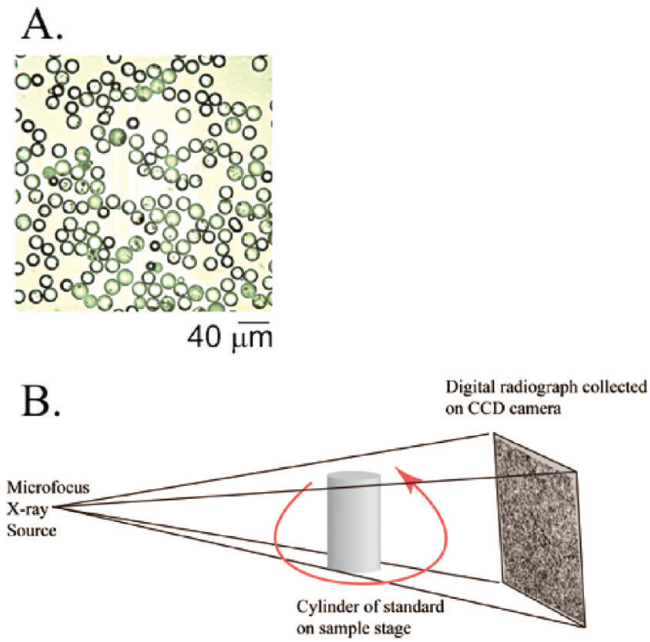

Figure 1. A. Image of NIST standard microspheres showing their uniform surface and geometry, B. Cartoon of the geometry of the Xradia μCT instrument showing the linear arrangement from the source to the scintillator with the sample in the middle on a rotation stage.

0.13 g divinylbenzene (both Sigma-Aldrich) was added to a gastight syringe. Approximately 100 mg of the silica microspheres was dispersed in 8 mL of water containing 1.5 mg/mL potassium persulfate (Sigma-Aldrich) by bath sonication (ca. 5 min). Immediately after sonication, the aqueous mixture was loaded into a second gastight syringe. The two syringes were joined and the phases were mixed by repeatedly exchanging the materials between syringes. A viscous emulsion was formed on mixing ca. 5 min. The mixture was then polymerized at 60 °C overnight. Water, catalyst, and emulsifier were removed by Soxhlet extraction, first with water for 4 days and then methanol for 48 h. Finally, the ~30 mg/cm^3 polystyrene foams were air-dried overnight.

The sample was imaged in 3D nondestructively using an Xradia (Concord, CA) μCT instrument. This instrument uses a Hamamatsu microfocus X-ray source with a tungsten target anode, which operates from 40−150 kV and up to 10 W with a spot size of 5 μm and a 43° cone angle. The source was operated at 40 kV and 4 W for these samples. The transmitted X-rays impinged on a scintillator mounted on one of the microscope objectives, which converted the X-rays to visible light. The visible light is imaged using the 2 × 2 k camera, Figure 1B. This instrument utilizes four objectives, 2×, 4×, 10×, and 20×. For these studies, the 4× and 20× objectives were used. For the 20× objective, pixel size of the sample at the detector under these conditions is 0.595 μm with a total field-of-view of ~1 mm. These conditions may be slightly altered by varying the source and the detector distance from the center of sample rotation. For each of the samples, a 60 s X-ray exposure was collected as the sample was rotated from −91° to +91°. The total number of radiographs collected included data sets of 181, 361, 721, and 1261 images. These represent total imaging times of 3, 6, 12, and 21 h, respectively. The data sets were sequentially acquired without removing the standard from the instrument; an identical area was imaged for each data set.

(19) Weber, E.; Fernandez, M.; Wapner, P.; Hoffman, W. *Carbon* **2009**, *48*, 2151–2158.
(20) Calvo, S.; Beugre, D.; Crine, M.; Leonard, A.; Marchot, P.; Toye, D. *Chem. Eng. Process.* **2009**, *48*, 1030–1039.

The polymer foam sample was imaged using the 4× objective, 721 images, and 80 kV and 4 W power. Using a lower resolution objective increases the X-ray flux on the scintillator; only a 25 s exposure was required. After reconstruction the foam pixel size is 5.33 μm with voids between 1 and 200 pixels wide with a mode of ~20 pixels wide. A higher kV (80 instead of 40) was needed for the polymer foam in order to achieve better penetration of the X-rays through the denser sample.

Three dimensional reconstructions were generated using Xradia XMReconstructor (version 7.0.2817), Xradia's proprietary reconstruction software. Reconstruction conditions included binning the data by a factor of 2 in all three dimensions to produce a final voxel size of 1.190 μm in all three directions and a data cube of one gigavoxel. The reconstructed slice data was directly exported as a series of tiff images.

The exported reconstructed slice data were read directly into AvizoFire 6.2 running on a 64-bit Hewlet-Packard computer utilizing an NVidia FX5800 graphics card with 4 GB of onboard RAM. Upon importing, the data was cropped to convert from a cylindrical data set to a cube. A threshold was applied which binarized the data (microspheres = 1, foam = 0). Next, a border kill command removed any objects that touch the surface boundary (removing incompletely rendered microspheres), and then an object separation filter is applied. It separates microspheres that may be touching. Finally the microspheres are analyzed including counting each microsphere's calculated volume and position. Statistics can then be exported to Origin for analysis, including converting the volume of each microsphere to a normalized diameter (assume each microsphere is a perfect sphere) and generating a histogram of the microsphere diameter distribution, microsphere calculated diameter and percent relative standard deviation. The calculation of the void size in the foam follows the same pattern except that at the binarization step, the voids (air) are given a value of 1, and the foam material a value of 0.

RESULTS AND DISCUSSION

Several of the steps between moving from a radiographic series of images to a 3D image with the reconstructed slices to the final statistics of the features of interest require user input. This can create significant variation in the final calculated statistics. Initially, when performing the reconstruction, the minimum and maximum pixel gray scale values of the reconstruction plane must be set. For example, using the 20× objective on the 20 μm beads for 181 radiographs, the maximum useful range of gray levels that covers all the features of interest is ~3000 counts. By contrast, for 1261 radiographs, ~15 000 counts is the useful range. There is a linear relationship with a $0.999 = R^2$ correlation between the number of radiographs collected and the useful gray level range. This indicates that the gray level sensitivity of the data is directly proportional to the number of images collected. In order to double the contrast, a doubling of the number of radiographs collected is required. During reconstruction then, these gray values are expanded to 16-bit gray levels for all of the images. Obviously, as more radiographs are collected, a larger difference in absorbance between matrix and the microspheres is possible. Figure 2 shows a sample reconstructed slice from each of the data sets, A-, B-, C-, and D-, corresponding to 1261, 721, 361, and 181 radiographs collected, respectively. As can be seen by these images, the noise level increases and the brightness of the particles decreases with decreasing number of radiographs collected. Separating the bead signal from the background noise becomes trivial for 1261 and 721 images, Figure 2.

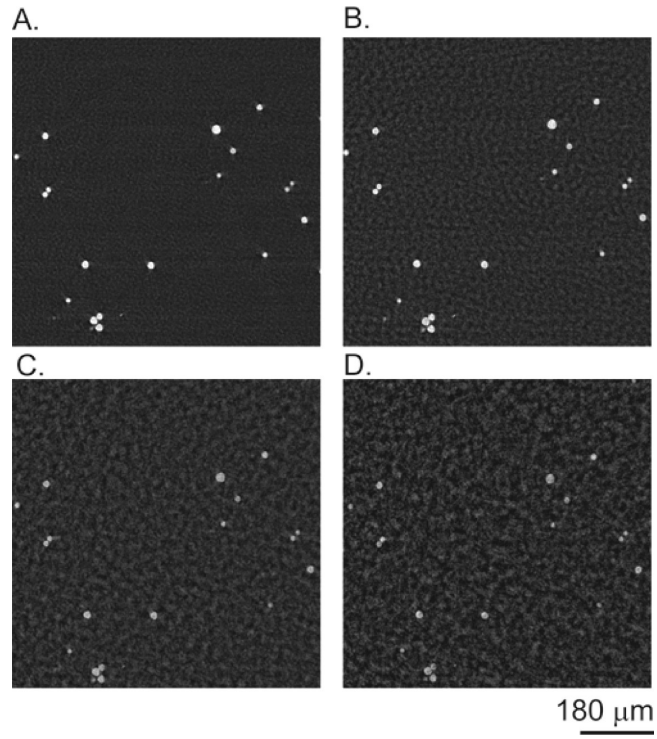

Figure 2. Individual slices from each of the data sets of 1261, 721, 361, and 181 images A−D respectively.

Second, when converting the image from gray scale to binary, a threshold must be set. Threshold directly influences the noise observed in the reconstructed images. For the high quality 1261 and 721 radiograph data sets, setting the level is simple. There is enough differentiation between the sample and the noise that a wide threshold range from which a single value can be easily chosen to capture the microspheres with minimal noise in the binary image. Noise appears as extraneous red dots in the binary image. Figure 3 overlays the gray scale images with the binary images for 1261 and 181 radiographs. There are almost no extraneous red, or binary dots for the 1261 radiograph image in Figure 3A but there are many spread about the 181 radiograph image, Figure 3B.

In addition to tracking noise, thresholding can influence imaging of the edges of a feature. For example, the trio of beads in the bottom left corner are blending together in the Figure 3A indicating a threshold too high was chosen, but the beads are separated in the 181 radiograph slice, Figure 3B, indicating a threshold too low was chosen. For each of the images, 181, 361, 721, and 1261, the binary threshold was set to 31 000, 34583, 25165 and 21 000. The variation in the selected threshold value corresponds to the variation in the reconstructed gray levels that were chosen. There is a clear inverse trend in the available threshold (above the noise) versus number of radiographs.

Histograms of the normalized diameter (converting the calculated volume of each object and assuming perfect sphericity) are presented in Figure 4. These histograms show two peaks in normalized diameter. One corresponds to the likely average diameter of the microsphere and the other to smaller volumes

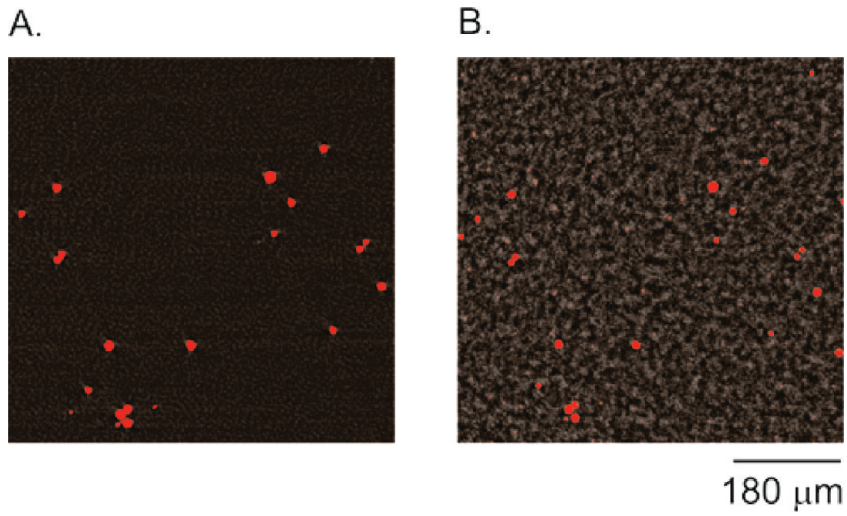

Figure 3. Same individual slice as in Figure 2 showing the threshold level applied to a reconstructed slice after collecting 1261 (A) and 181 (B) images. With a decrease in the number of images the overall noise increases as seen by the single pixel noise points. Note that the bead diameter decreases as seen by the separation of the three neighboring beads on the bottom left.

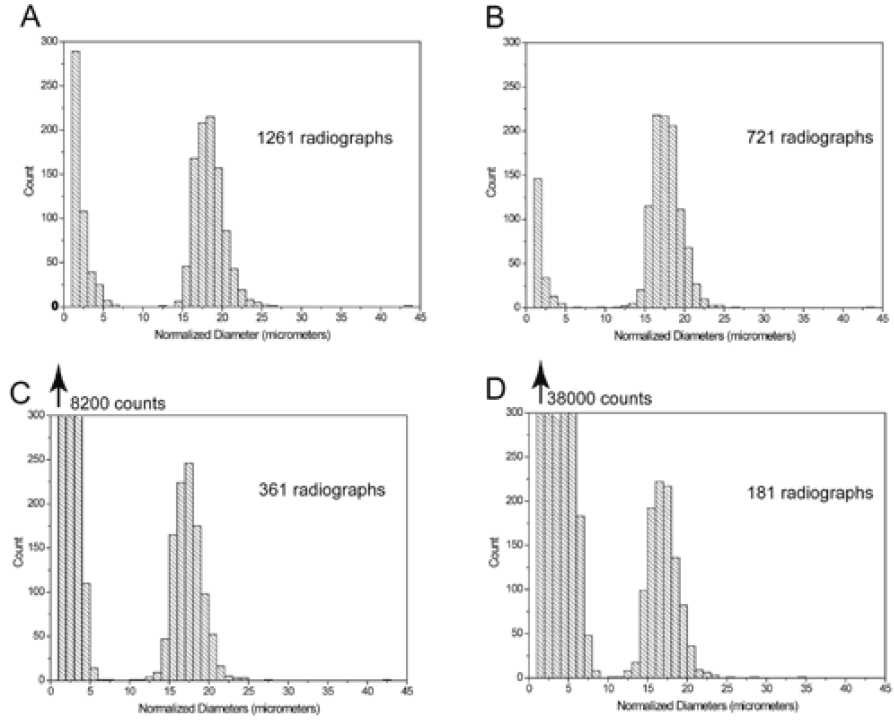

Figure 4. Histogram plots of the normalized diameters of each individual binarized object in the 3D image. Increasing the number of radiographs increases the separation in the noise versus pixel noise and the overall pixel noise decreases for the four data sets, 1261, 721, 361, and 181 radiographs, A-D respectively. Note that the noise in C and D is off scale.

that are likely noise within the thresholded image. When examining these histograms, the first couple of columns are voxels of $1 \times 1 \times 1$ pixels and then $1 \times 1 \times 2$ pixels and the graph continuously increases in this manner. These small voxels are those that were captured during the threshold process and are noise in the binary image. It should be noted that choosing the threshold value is much more difficult for the lower quality 361 and 181 radiograph images where the noise values and the microsphere values are much closer, shown in Figure 4C and D. A low enough threshold value must be found to capture the entire volume of the microsphere, but minimize the noise in the rest of the image. In some of the microspheres of the 181 radiograph data set, there is binary noise which reduces the volume calculated, interior voxels that drop out. As can be seen by Figure 4D, the noise in the binary data set is large so a careful balance is difficult to achieve.

Finally, the third user input that is important to the analysis of the CT data is the selection of the parameters to separate the microspheres. If two spheres are closer than the resolution of the data set, two spheres may be rendered and counted in binary as one object. A separation routine can be applied to separate them. Again, a value must be chosen that separates without slicing solid

Table 1. Average Bead Diameter for The NIST Standard As Calculated by 3D μCT and Their Relative % Standard Deviation

	NIST standard	1261 radiographs	721 radiographs	361 radiographs	181 radiographs
average bead diameter (μm) and SD	17.3 ± 1.4	18.4 ± 1.9	17.8 ± 1.9	17.4 ± 1.9	17.0 ± 1.9
relative % SD	12	10.7	10.8	11.1	11.2

spheres apart. Data for the 1261 radiograph image was chosen and the binary image was separated with values of 1, 2, 3, and 4 pixel wide depth of valley. A separation value of 2 was chosen for all four of the microsphere data sets.

Once the inputs are all selected, characteristics of the feature of interest can be determined, in this case the diameters of the microspheres. Results of the calculated diameters of the microspheres are given in Table 1. The 1261 radiographs data set was used to set the threshold between microsphere and noise, a threshold of 10 μm diameter was used in calculating the microsphere volume for all the data sets. All objects below 10 μm were considered noise; however, there is one anomalous microsphere in the data sets that is approximately 43 μm in diameter, and its calculated diameter drops with decreasing number of radiographs. Setting this 10 μm minimum is simple for the 1261 radiograph data set and is fully justified by the histogram of the diameter of the microspheres. In a real-world sample where the distribution of the size range is not so tight, operators will not have the luxury of determining where the noise cutoff is located and will be required to integrate all binary voxels. Therefore, it becomes

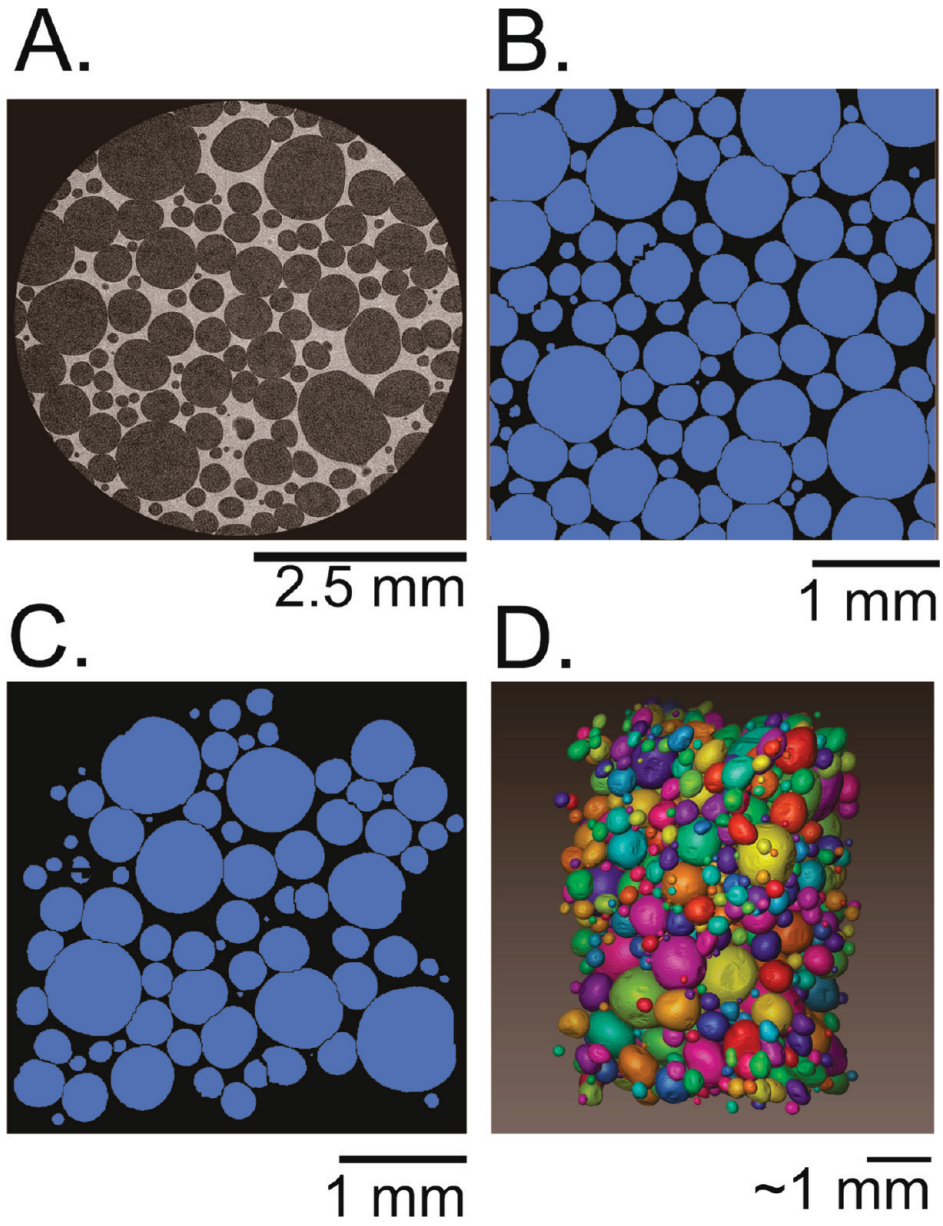

Figure 5. Raw reconstructed slice of the polymer foam (A), after binarization, image crop and void separation (B), after removal of edge objects (C), and labeled 3D image of interior voids (D).

paramount to reduce the noise in the binary image as much as possible by acquiring the appropriate number of images. Collecting at least 721 radiographs appears to do this. The average diameter and %RSD statistics show that the microsphere measurements meet the statistics given in the certificate for all data sets with a clear downward trend in the calculated size and a clear upward trend in the %RSD when both values are compared to the number of radiographs. However, discriminating microspheres versus noise is much simpler for the 1261 and 721 radiographic data sets. The statistics for the 1261 and 721 radiograph data sets indicate microsphere diameters greater than the NIST standards indicating that the subjectivity of choosing the threshold value needs to be removed. Too few radiographs causes noise to dominate and resolution to degrade resulting in an inaccurate capture of the microsphere shape. Too many radiographs, and the data collection time becomes inappropriate.

To test the applicability of the calibration or standardization technique developed in the microsphere analysis, a 3D reconstruction of a polymer foam was conducted and data treatments similar to the microspheres applied. A reconstructed slice through the polymer foam is given in Figure 5A. In order to bring the exterior surface of the data set into the foam, the data was cropped from a cylindrical data set into a cube. After cropping and binarization, the binary separation algorithm separated the foam voids as shown in Figure 5B. Using the total binary volume (total void volume), 48.0 mm^3 out of the total data cube volume, 62.0 mm^3, the void fraction of the sample is calculated to be 77.3% voids. The average void size was calculated to be 280.1 μm diameter however this incorrectly included all voids that touch the data cube surface and may only be partially rendered. A more correct approach is to remove all voids that intersect the cube surface (Figure 5C) which produces a more accurate average void diameter of 274.4 μm. While this is an average diameter difference of 2%, in volume it represents a more significant 6%. Finally, Figure 5D is a labeled image of the interior voids. The coloring is simply to aid in differentiating between voids. Rough areas on the surface of the rendered voids are locations where voids were intersecting other voids that have been removed in the border kill step of the data processing. Now it is possible to physically measure the void sizes, distribution of the sizes, orientations, size with respect to location such as void size changing near the surface of the foam, as well as the void aspect ratio and Feret diameters (which is the maximum diameter of the sample as if measured using calipers). With these techniques, comparing formulation results, aging changes, locations within a part or batch and changes due to loading are quantifiable. The use of a 3D dimensional standard to confirm the performance of the instrument, provides the confidence in the statistics of samples with features of unknown size that their measured values can be trusted. Although the microspheres are more than ten times smaller than the voids, the standard is directly applicable as the lower limit of the resolution of the instrument, therefore with the confidence that the instrument can measure these accurately, the measurement of large features become trivial. This standard will also be useful independent of the material assuming proper X-ray penetration and can be useful for glass microcapsules embedded in a polymer or metallic particles in an aerogel foam.

CONCLUSIONS

The quality of a 3D reconstruction of μCT data is a function of many parameters. These parameters include the signal-to-noise of the individual radiographs, dimensional accuracy[8] and contrast of the radiographs, number of radiographs, noise minimization during acquisition (e.g., ring artifacts) and reduction of beam hardening. Also of importance is the quality of the reconstruction algorithm. Most of these parameters are inherent to an individual instrument but several require the knowledge and experience of the operator and the selection of the right filters, acquisition settings and time on the instrument, specifically dwell time and number of radiographs.

Due to the utility of 3D μCT in examining and quantifying defects, voids, and particles in cast parts, foams, and particle dispersions, optimizing and confirming the dimensional performance of the instrument is paramount. A simple 3D size standard that can be made without the need for expensive equipment and that can be tailored to fit many applications and size scales based upon NIST standard microspheres embedded in low density poly(styrene) was utilized. Three-dimensional data processing software is required to achieve the desired scale calibration.

Measuring this size standard has found that the more radiographs collected, the greater the dimensional accuracy and the lower the measured %RSD, which was not unexpected. While all four data sets measured the microspheres within the specifications given by the manufacturer, at lower numbers of radiographs, image noise dominates. For these "perfect" samples where the feature size is known even before analysis, setting the size threshold in order to obtain the correct statistics and remain out of the noise region is trivial. In a "real" sample with unknown feature sizes no such knowledge is available before analysis. Setting the size threshold to avoid noise domination is very difficult but must be optimized. The way to do this is to collect enough images to minimize the noise. From this work to best obtain the high contrast between the microspheres and the polymer binder as well as minimize image noise, 721 images appears to be adequate to accurately measure these small high contrast objects. More images are needed if the contrast between objects are similar in X-ray absorption. Therefore this standard can be tailored for samples with lower X-ray contrast by varying the density of the polymer used to embed the microspheres. For the current study a density of ~30 mg/cm^3 poly(styrene) foams were used which allowed for a very high X-ray contrast. Depending upon the sample that needs to be calibrated for, a higher density poly(styrene) foam can be used, up to about 500 mg/cm^3, or another foam material such as silicone (with the same elemental species as the microspheres), which lowers the contrast between the features of interest and the matrix. As the gray scale range is directly proportional to the number of radiographs collected, more radiographs would be required to increase the contrast.

Future work will include determining the appropriate exposure times required, although 1 min appears, for this study, to be more than adequate. Of even more importance, a rigorous method for determining the threshold values for samples must be found. Also of interest, will be size standards in materials of similar X-ray contrast as well as using a dispersant of higher X-ray absorption to effectively manufacture "voids". Applications of the lessons here

will be used to measure the statistics of voids in foams from various formulations and exposed to various conditions as well as examining the 3D structures in metals damaged due to dynamic loading.

ACKNOWLEDGMENT

LANL is operated by LANS, LLC, under DOE/NNSA contract DE-AC52-06NA25396. We acknowledge Andrew Dattelbaum for providing the microspheres, Trevor Marks for the foam sample, and George J. Havrilla and Ellen Cerreta for their technical feedback. Funding was provided by the Laboratory Directed Research and Development program (LDRD-DR's 20080015 and 20100026) as well as the Institute for Multiscale and Materials Studies.

Received for review June 8, 2010. Accepted August 31, 2010.

AC101522Q